J Mater Sci (2010) 45:233–241
DOI 10.1007/s10853-009-3925-6

# Pyrolysis of aluminium loaded polymethylsiloxanes: the influence of Al/PMS ratio on mullite formation

**Juliana Anggono · Brian Derby**

Received: 22 April 2009 / Accepted: 23 September 2009 / Published online: 14 October 2009


**Abstract** Al-filler-loaded polymethylsiloxane (PMS) was pyrolysed in air atmosphere at temperatures 400–1700 °C. The effect of the Al amount added to the PMS on phase development, densification behaviour and microstructure evolution was studied by simultaneous thermal analysis, X-ray diffraction, scanning electron microscopy and electron probe microanalysis. The Al/PMS reaction route is complex producing Si, $SiO_2$ (amorphous and cristobalite), $Al_2O_3$ ($\gamma$-, $\iota$- and $\alpha$-$Al_2O_3$), $Al_2OC$, $Al_4O_4C$, $Al_4SiC_4$, and AlN, depending on the ratio of Al/PMS in the initial mixture. Increasing the Al content (high Al/PMS ratio) reduces the amount of voids and porosities after PMS degradation. The voids and porosities provide access for the oxygen atmosphere into the inner structure to oxidise the Al particles, Si or SiC and also as channels for the PMS degradation products to escape. Mullite formation was identified in sample containing >73 wt% Al at temperature as low as 1400 °C.

## Introduction

The pyrolytic degradation of preceramic polymer precursors can result in a series of complex, thermally induced processes, which yield condensed ceramic and gaseous reaction products. The release of gaseous species leads to shrinkage and porosity generation. Adding reactive powder to the preceramic polymers results a series of reactions between the powder and the amorphous ceramic residue or gaseous species. Reaction with the gas either from the atmosphere or from the pyrolysis product of the polymer is facilitated by high preform porosity, which provides easy access to the reaction site [1, 2].

This process has been used successfully to produce mullite with aluminium as the active filler and polymethylsiloxane (PMS) [3–5] or polydimethylsiloxane (PDMS) [6] as the preceramic polymer. Phase and microstructure evolution in these systems has been explored using thermal analysis and X-ray diffraction (XRD) [6], and these in parallel with electron probe microanalysis (EPMA) [4, 5]. This prior work has shown that the formation of mullite occurs by the parallel oxidation of the siloxane polymer and the metal to form $Al_2O_3$ and (mostly) amorphous $SiO_2$ that react together at high temperature to form mullite. However, the siloxane oxidises at a lower temperature than does Al and hence a stage occurs where the Al reduces the siloxane, or its oxidation product, to elemental Si at intermediate temperatures [4, 6]. The morphology of the Al particle-filled preceramic polymer body was found to be of key importance [5]; with the size and shape of the Al particles controlling pore structures at intermediate temperatures and this strongly influencing the access of oxygen to the compact and hence the final composition after heat treatment.

Mullite crystal structure materials have the general formula $Al_{4+2x}Si_{2-2x}O_{10-x}$ and it has been stated that, from a structural point of view, mullite should exist in a full composition range from $x = 0$, which gives 50 mol.% $Al_2O_3$ (sillimanite), to $x = 1$, which gives 100% $Al_2O_3$

J. Anggono · B. Derby
School of Materials, University of Manchester,
Grosvenor Street, Manchester M1 7HS, UK

J. Anggono (✉)
Department of Mechanical Engineering,
Petra Christian University, Jalan Siwalankerto 121-131,
Surabaya 60236, Indonesia
e-mail: julianaa@petra.ac.id

(ι-alumina). [7, 8] However, it is observed that mullite-like crystal structures with compositions at low values of $x$, such as sillimanite and andalusite, only form under high pressures. Under normal atmospheric pressure, mullite produced by solid-state reaction normally has a composition in the range $0.25 < x < 0.4$, which are often referred as 3:2 and 2:1 mullite from their respective $Al_2O_3$:$SiO_2$ ratios. Fischer et al. were able to extend the range of mullite compositions to values of $x > 0.8$ using sol–gel synthesis [9]. To date, published studies on the formation of mullite from Al-filled polymer precursors have studied compositions that produce stoichiometric (3:2) mullite [3–6]. Scheffler and Greil studied the effect of different concentrations of Al reactive fillers on the composition of pyrolysed of siloxane polymers after heat treatment up to 1000 °C [10]. They found that the fraction of the initial carbon retained after pyrolysis increased with increasing Al content. However, the pyrolysis temperature studied in their work was too low to nucleate mullite. In this study, we report on the effect of Al filler content on the reaction sequence and final products during the pyrolysis of Al-filled PMS at temperatures up to 1700 °C. Possible mullite compositions with $x = 0.4$ or lower have been selected.

## Experimental procedure

The starting materials were PMS (0009465, Wacker Silicone Resin MK, Wacker-Chemie, Germany), a solid thermosetting siloxane polymer used as a $SiO_2$ precursor and Al as the filler component (27064 4Y, Merck Chemicals, Poole, UK). PMS is solid methyl silicone resin which predominantly inorganic: only 11 wt% is thermally degradable organic content; the rest is pure silicon dioxide (after complete oxidation: approximately 82% $SiO_2$ is obtained). Its average molecular weight is 2,000 to 6,000 g/mol. The resin has the basic components of oligomeric methyl polysiloxanes. Additionally, these oligomers contain a few mole-percent of reactive ethoxy (–$OC_2H_5$) and hydroxyl groups (–OH) which release water and ethanol as by-products during curing. The Al flakes were plate like with a thickness <1 μm and diameters in the range 30–60 μm, they had a high level of oxidation and had oxide films ≈30 nm thick. The only significant metallic impurity was Fe at a concentration <0.5%.

Samples were prepared by dissolving the PMS resin in an ethanol:acetone mixture, ratio of 95:5 vol%, to which the Al powder was mixed by manual stirring at Al contents of 73, 64, and 51 wt% with respect to PMS and Al total; these were designated B1-A, B1-B and B1-C, respectively. The nominal mullite composition that each sample designation would achieve is indicated in Table 1, these compositions should be taken as a guide because of the uncertain thickness of the oxide film. Aluminium acetylacetonate (Sigma Aldrich, Poole, UK), at 1 wt%, was added as a catalyst. After evaporating the solvent by leaving the mixture in the fume cupboard for ≈7 days, the subsequent blends were manually ground using a mortar and pestle before sieving through a mesh of 100 mesh size (≈150 μm) to form granules. This granulate was used to form green compacts by shaping in a steel die press at 200 °C and 15 MPa to cross link the polymer, yielding solid, dense cylindrical pellets of 16 mm diameter. Samples B1-A and B1-B were shaped into 2–3 mm thick pellets and sample B1-C 1.1 mm. Pyrolysis and high temperature heat treatment were performed in air in a conventional chamber furnace. Following our earlier work [4, 5], the heat treatment was as follows: heating to 700 °C at 10 °C $min^{-1}$, followed by an isothermal hold for 2 h to oxidise the polymer; heating to 1200 °C at 10 °C $min^{-1}$, followed by another isothermal hold for 10 h to convert the Al to the corresponding oxide; followed by a final heating ramp to 1700 °C at 10 °C $min^{-1}$ with 4 h isothermal hold to allow the formation of mullite. Samples were removed from the furnace at different temperatures within this heat treatment cycle and then cooled in air to room temperature. These samples were then used for further analysis to determine the sequence of intermediate products and reactions leading to the anticipated formation of mullite.

**Table 1** Composition of starting material and ideal oxide ratio after oxidation reaction

| Sample designation | B1-A | B1-B | B1-C |
|---|---|---|---|
| Wt% Al flake | 73 | 64 | 51 |
| Molar % Al | 86 | 80 | 70 |
| Molar % Al with 50 nm oxide film | 85 | 79 | 69 |
| Nominal ratio $Al_2O_3$:$SiO_2$ | 3:1 | 2:1 | 3:2 |

Phase analysis was conducted by XRD using Cu $K_\alpha$ radiation (PW3710 diffractometer, Philips, Eindhoven, Netherlands). The sequence of reactions was monitored using simultaneous thermal analysis (STA) consisting of thermal gravimetric analysis (TGA), differential scanning calorimetry (DSC) (STA 449C, Netzsch, Germany) and evolved gas analysis (EGA) (Thermostar GSD 300 T, Balzers, Lichtenstein). The resulting chemical composition and microstructures obtained after heating the Al/PMS mixtures were investigated by scanning electron microscopy (SEM) (6300, JEOL, Tokyo, Japan and SEM525, Philips, Eindhoven, Netherlands) and by EPMA (SX100, Cameca, Paris, France) using energy dispersive spectroscopy (EDS) and wavelength dispersive spectroscopy (WDS).

## Phase and microstructure evolution

### Thermal analysis

Figure 1a shows the simultaneous DSC and TGA traces obtained from the 3 Al/PMS blends heated to 1600 °C. An earlier STA study of Al/PMS mixtures and of the constituent Al particles and PMS in isolation, identified a number of characteristic features (numbered on Fig. 1a) [4]. Point 1 is associated with cross-linking reactions in the PMS and has an associated evolution of $H_2O$, ethane and $CO_2$ identified by EGA (Fig. 1b). Point 2 is an exotherm linked to the degradation of PMS and is accompanied by intense $H_2$ and $H_2O$ signals with weaker $CO_2$ and ethane signals on the EGA trace. Greil et al. [11]. and Renlund [12] found that the pyrolysis of PMS produces methane ($CH_4$), hydrogen ($H_2$), and free carbon (C), as well as other products. Schmidt et al. [13] suggested the ethane ($C_2H_6$) could possibly be the side product of the methane reaction at $T > 600$ °C. Point 3 indicates oxidation of Al in the solid state, as can be seen by the accompanying weight gain on the TGA; the sharp endotherm (4) identifies onset of melting of the Al particles. Points 5 and 6 on the DSC are also associated with weight gain on the TGA trace indicating the liquid state oxidation of Al. The sharp endotherm around 1400 °C, seen in sample B1-C, indicates the melting of elemental Si, which has been produced by a redox reaction between the Al and the PMS or its oxidation product [4]. Sample B1-C also shows some DSC exotherms at higher temperatures, these may be associated with solid-state reactions leading to mullite formation. Note that as the Al content of the mixture increases (A > B > C), many of the exotherms shift to lower temperatures. This was also reported earlier when comparing the exotherms in PMS-Al mixture with those observed in PMS and Al tested in isolation, where the presence of PMS was seen to shift the oxidation exotherms associated with Al to higher temperatures [4].

### Phase characterisation

Figure 2 shows XRD traces taken from the three samples after heat treatment to a range of temperatures; note that the specimen heated to 1200 °C was held at that temperature for 10 h, while the other specimens were removed from the furnace once they reached the stated temperature. The results are similar to those reported in our earlier studies [4, 5]. The oxidation of PMS at low temperatures does not form any identifiable crystalline phases and the higher temperature oxidation of Al results in the formation of α-alumina. This is different from the results of Michalet and co-workers who reported a sequence of transition aluminas on oxidation of much finer Al powder fillers. In all three samples, elemental Si appears at 1000 °C, note that only specimen B1-C had shown a Si endotherm during STA. The formation of Si during the heat treatment of Al/PMS and PDMS/Al has been reported earlier [4, 6] and is believed to be the consequence of a redox reaction between liquid Al and the oxidation product of the PMS. It was also earlier hypothesised that such a redox also contributes to the formation of SiC in specimen B1-C [4]. In specimens B1-A and B1-B, it is proposed that the greater Al excess suppresses the formation of SiC and instead any free C reacts to form the aluminium oxycarbides identified on the respective XRD traces in Fig. 2a and b. At higher temperatures in the heat treatment the difference between

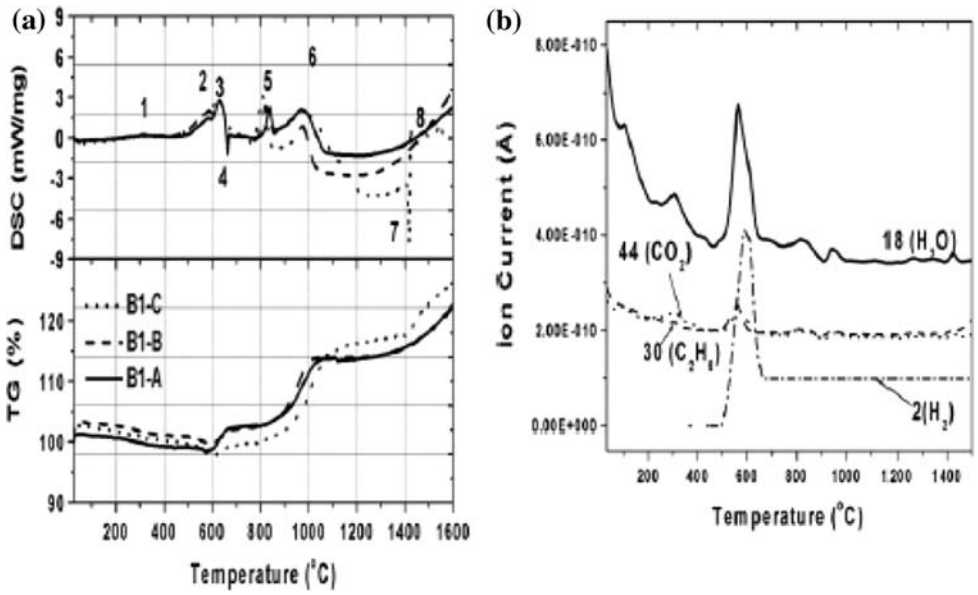


**Fig. 1** **a** STA traces (DSC and TGA) of PMS/Al samples B1-A, B1-B and B1-C heated up to 1600 °C with a heating rate of 10 °C $min^{-1}$ in air. **b** EGA traces from sample B1-C

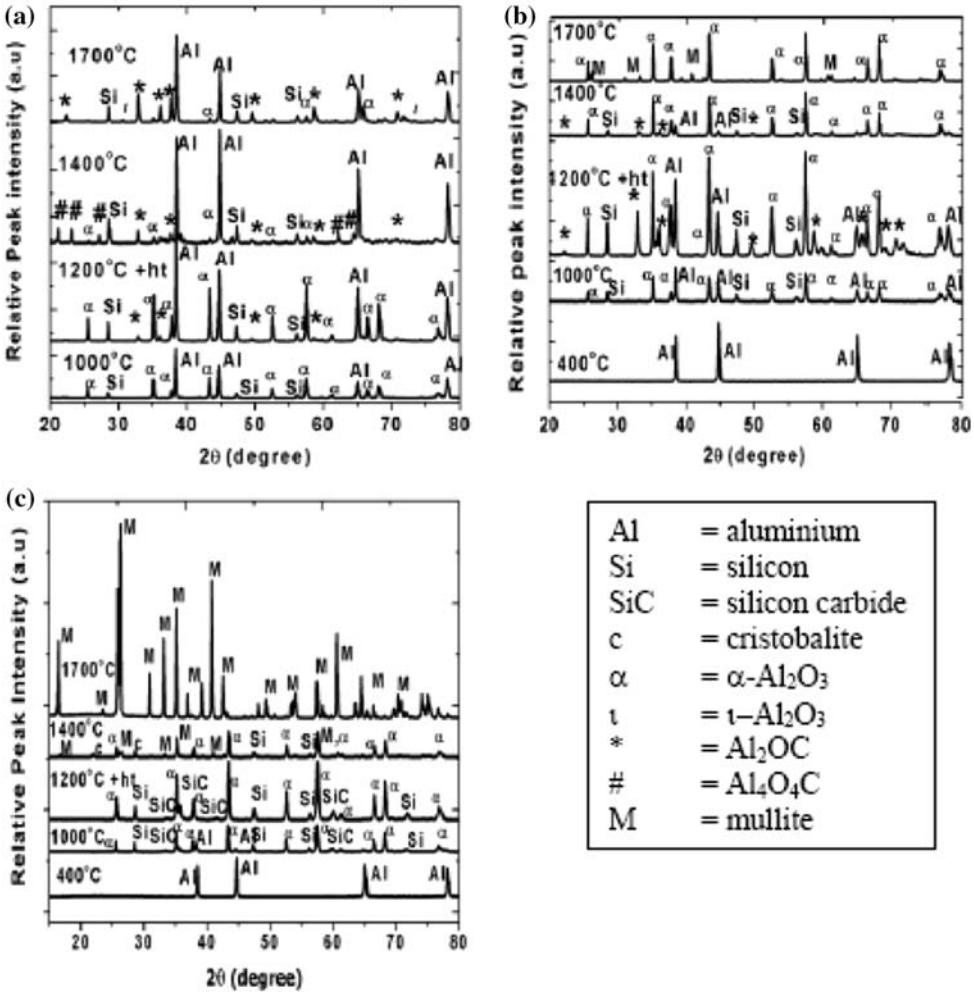


**Fig. 2** XRD traces taken from samples **a** B1-A, **b** B1-B and **c** B1-C after various heat treatment temperatures; showing phase development at different temperatures (+ht = 10 h holding time)

the three compositions becomes greater. Only sample B1-C shows mullite and no other crystalline phases at 1700 °C, B1-B shows a mixture of α-alumina and mullite, whereas B1-A shows large quantities of retained Al, strong Si and $Al_2OC$ traces and relatively weak α-alumina. In B1-A, there is a weak signal in the 1700 °C XRD trace that could be identified as ι-alumina but the signal is too weak to be conclusive.

In order to study some discrepancies between the STA and XRD data, XRD analysis was carried out on the residue in the STA pan after the thermal cycle for specimens B1-A and B1-C. The residue from B1-A contained free Al and Si together with α-$Al_2O_3$. The B1-C residue contained mullite with Si and α-$Al_2O_3$. Complete oxidation of Al was achieved as no free Al was identified in B1-C. The STA residue had a maximum thermal exposure of 1600 °C and thus it cannot be directly compared with the 1700 °C XRD traces shown in Fig. 2. However the absence of free Al in B1-C is consistent with Fig. 2, which showed no Al in the 1400 or 1700 °C furnace treated sample. The presence of free Si in the STA residue of specimen B1-A, despite the absence of a clear Si melting endotherm in Fig. 1a probably indicates the lower sensitivity of the STA to signals from small concentrations of components.

## Evolution of microstructure

The evolution of microstructure during the thermal treatment of Al/PMS mixtures with nominal composition such as to produce 3:2 mullite (i.e., compositions identical to sample B1-C) have been reported in detail elsewhere [4, 5]. Here we concentrate on the high Al content mixtures and report on the results from stoichiometric compositions solely for purposes of comparison.

During the early stages of processing the intermediate microstructures are defined by the starting materials. Figure 3 shows backscattered electron (BSE) images obtained by SEM examination of samples B1-A and B1-C after heat treatment to 400 °C. The lower PMS content in B1-A results in a lower porosity structure with larger and more numerous voids than seen in B1-C, which is almost completely dense. In both cases, there appears to be good

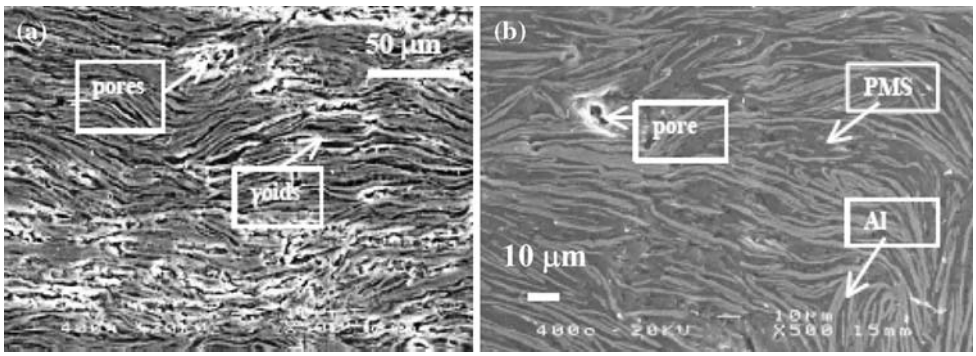


**Fig. 3** SEM BSE images of sample **a** B1-A and **b** B1-C after heating to 400 °C

mixing of polymer and filler resulting in a homogenous microstructure. The microstructure shows strong orientation induced by the Al particle morphology during the pressing stage. On heating to higher temperatures, the strong influence of the initial microstructure as determined by the Al flake morphology is clearly still evident in all three samples (Fig. 4). On further examination of the microstructures in Fig. 4, we can see significant differences between the specimens, especially near the free surface or the surfaces of internal voids. Specimen B1-C, which has the Al/PMS ratio determined to produce 3:2 mullite shows the most homogenous microstructure with little obvious variation towards the surface visible at the top of the image in Fig. 4f. However, both B1-A and B1-B show a strong influence of the surface on the microstructure after heat treatment. Both these samples are Al rich but they show quite distinctly different surface structures. B1-A shows a dense surface region and from the grey contrast in the BSE image showing lower atomic number density this is identified as containing $Al_2O_3$ (this was confirmed by EDS microanalysis) at 1400 °C and leading to an almost continuous $Al_2O_3$ surface layer at 1700 °C. The specimen centre shows a slightly lighter contrast, tentatively identified with a high Al content, the bright white regions may indicate elemental Si and this will be investigated further by EPMA. In contrast sample B1-B shows a highly porous surface morphology (this is also evident near the surface of the large void in the centre of Fig. 4b). The low magnification of the images of B1-B results in a poor separation of phases in the images and this will be studied further using EPMA. From this we can confirm that the large light regions in Fig. 4c are indeed large flakes of elemental Si and the elongated particles in Fig. 4f are mullite.

Figure 5 shows EPMA elemental maps obtained from specimens B1-A and B1-B after heat treatment in air to 1400 °C. In both cases, the specimen surface is included at the bottom of each image. Note that the colour scales in B1-A and B1-B are not directly equivalent. In both specimens the EPMA images confirm the observations made concerning the BSE images in Fig. 4. In specimen B1-A,

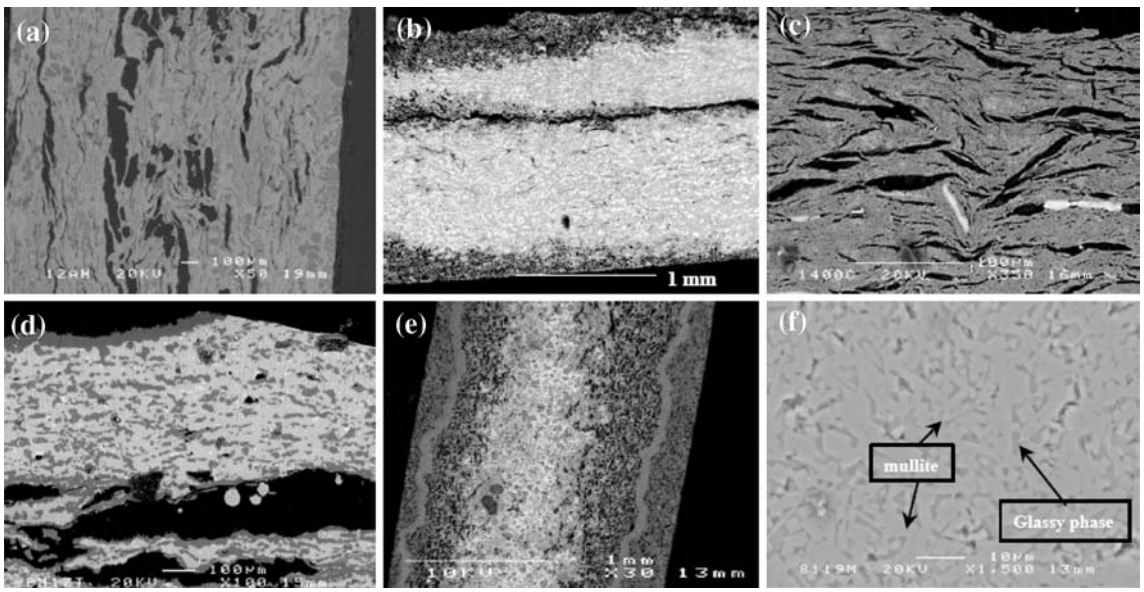


**Fig. 4** BSE SEM images after heat treatment to 1400 °C: **a** B1-A, **b** B1-B, **c** B1-C, and after heat treatment to 1700 °C, **d** B1-A, **e** B1-B, **f** B1-C

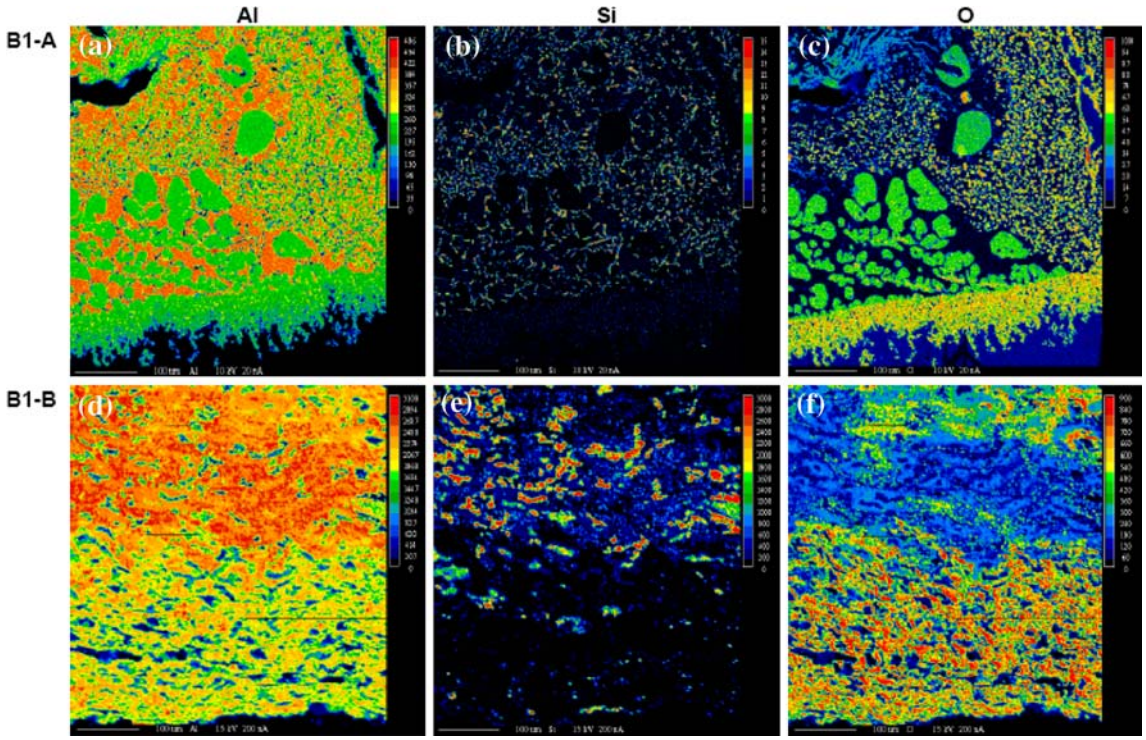


**Fig. 5** EPMA elemental maps from filled PMS specimens after heat treatment to 1400°C: B1-A **a** Al, **b** Si, **c** O and B1-B **d** Al, **e** Si, **f** O. In each case, the scale bar represents 100 μm

the green colour of the Al map coincides with green on the O map and an absence of Si to indicate the presence of a continuous $Al_2O_3$ layer along the specimen surface. Immediately beneath this region are circular sections of $Al_2O_3$ surrounded by an Al rich matrix containing elongated regions of high Si content. Careful study of the elemental maps shows that the larger of these Si regions correlate with an absence of both an Al and an O signal, indicating elemental Si. In specimen B1-B the surface is also found to be predominantly $Al_2O_3$ with Si largely absent, although here it is a porous region. Immediately below this region of porous $Al_2O_3$ is a region that is rich in Al but contains large regions of elemental Si. Surrounding the Si flakes is a region in which Al and O signals are present but outside this region Al predominates.

## Discussion

The differences in phase evolution seen in samples B1-A through to B1-C are the result of the decreasing Al content of the mixture prior to heat treatment. From the nominal compositions of the starting materials given in Table 1, sample B1-C is expected to produce pure 3:2 mullite at equilibrium. Composition B1-B would generate a 2:1 mullite if it underwent perfect conversion. This is at the $Al_2O_3$ rich composition limit often assumed for the mullite produced by solid-state reaction. B1-A is outside the normally accepted composition limit for mullite but is in the range of compositions of mullite that have been reported as synthesised using sol–gel precursors [9].

Two types of Al-oxycarbide were formed ($Al_2OC$ and $Al_4O_4C$) besides Al, Si, $Al_2O_3$ in the lowest ratio (B1-A) and no mullite was detected by XRD up to 1700 °C. Similarly with the B1-B sample all the above traces were identified except the $Al_4O_4C$. A small quantity of mullite was detected at 1700 °C. Traces of Al-oxycarbide were not observed in the B1-C sample, but SiC and $SiO_2$ (cristobalite) peaks were found in the 1000 and 1400 °C samples, respectively. It was surprising to find $\iota$-$Al_2O_3$ at the relatively high temperature of 1700 °C (Fig. 2a) and also no indication of transition alumina polymorphs ($\theta$-, $\delta$- and $\gamma$-$Al_2O_3$) formed prior to formation of $\alpha$-$Al_2O_3$. Similar work using smaller Al particles (0.8 μm) mixed with PDMS found the formation of transition alumina polymorphs ($\theta$-, $\delta$- and $\gamma$-$Al_2O_3$) after heat treatment up to 1200 °C [6].

Heat treatment to temperatures below the melting temperature of Al is expected to lead to the gradual decomposition and oxidation of the PMS to an amorphous $SiO_2$ or Si–O–C matrix mixture. Oxidation of the Al will be relatively slow as is evidenced by the absence of detectable transition alumina. Above the melting point of Al, its

oxidation is accelerated by the disruption of the oxide film. The flow of Al can also lead to direct contact between Al and the oxidised Si rich matrix. In earlier work, we proposed a series of possible redox reactions between Al and the matrix that could result id the formation of Si or SiC [4]. Here we must also include those that could lead to the formation of the aluminium oxycarbide phases.

$$4\mathrm{Al} + 3\mathrm{SiO_2} \rightarrow 2\mathrm{Al_2O_3} + 3\mathrm{Si_{Al}} \quad (1)$$

$$4\mathrm{Al} + 6/(x-y)\mathrm{SiO}_x\mathrm{C}_y \rightarrow 2\mathrm{Al_2O_3} + 6y/(x-y)\mathrm{CO}\uparrow + 6/(x-y)\mathrm{Si_{Al}} \quad (2)$$

$$4x\mathrm{Al} + 6\mathrm{SiO}_x\mathrm{C}_y \rightarrow 2x\mathrm{Al_2O_3} + 6y\mathrm{SiC} + 6(1-y)\mathrm{Si_{Al}} \quad (3)$$

$$4(x+y)\mathrm{Al} + 3\mathrm{SiO}_x\mathrm{C}_y \rightarrow (x-4y)\mathrm{Al_2O_3} + 3y\mathrm{Al_4O_4C} + 3\mathrm{Si_{Al}} \quad (4)$$

$$4(2x+y)\mathrm{Al} + 6\mathrm{SiO}_x\mathrm{C}_y \rightarrow 2(x-y)\mathrm{Al_2O_3} + 6y\mathrm{Al_2OC} + 6\mathrm{Si_{Al}} \quad (5)$$

where the subscript Al represents Si in solution in liquid Al. Because of the uncertain composition of the $SiO_xC_y$, these reactions are necessarily schematic. We postulate that reactions 4 and 5 are favoured if there is a large Al excess. In which case the Si activity will be reduced, suppressing the precipitation of SiC and favouring the formation of $Al_2OC$ or $Al_4O_4C$. In all cases, the redox reactions result in elemental Si and this is consistent with the XRD and EPMA results. It has been proposed by others that $Al_2OC$ might be the result of a reaction between $Al_4C_3$ and $Al_2O_3$ [10–12]. Greil et al. and Renlund et al. suggested that $Al_4C_3$ results from the reaction between the metal filler and free C [11, 12] while Scheffler and Greil proposed that the formation of $Al_4C_3$ takes place at the melting point of Al when the Al melt reacts with methane gas ($CH_4$) [10]. No evidence is shown in our XRD data (Fig. 2) for the presence of $Al_4C_3$ prior to the appearance of the aluminium oxycarbide phases. XRD results (not shown) for specimen B1-B heated to 1200 °C without any holding time found the phase $Al_4SiC_4$, which could be evidence of the presence of $Al_4C_3$.

Figure 5 offers further evidence for the importance of redox reactions in specimen B1-A. At the surface, there has been significant oxidation of the Al and this may have prevented access of atmospheric $O_2$ immediately below this surface layer. The islands of $Al_2O_3$ below the surface are surrounded by matrix that is depleted in O. Indeed from the O map (Fig. 5c), the material surrounding the $Al_2O_3$ appears to be Al containing Si flakes, which would be in solution in liquid Al during heat treatment. This behaviour is not seen in B1-B (nor was it reported earlier in B1-C) [4] we postulate that this may be the result of the microstructure prior to firing. B1-A has a very low PMS content and as can be seen from Fig. 3a there are a large number of voids that will fill when the Al melts. In B1-B and B1-C, the higher PMS content leads to this space being filled with pyrolysed polymer (Fig. 3b). Thus there is reduced access of atmospheric $O_2$ to promote the oxidation of the Al and redox reactions dominate.

In Figs. 4 and 5, it can be seen that specimen B1-B has a highly porous surface region that is deficient in Si. Very similar structures have been reported in an earlier paper that studied the effect of Al filler particle morphology on the pyrolysis of Al/PMS mixtures [5]. In this study, it was found that if a fine spherical Al powder was used, oxygen access to the specimen centre was impeded and Si loss occurred from the surface. The volatile compound SiO can form under reducing conditions and that could be one mechanism for the observed loss of Si from the surface regions. Suttor et al. who first studied the decomposition of Al-filled PMS also observed the evolution of volatile SiO as an additional minor loss in the temperature range of 700–1200 °C [3]. In order to further explore the difference between the inner and surface regions of the specimens, XRD data were obtained from B1-B and B1-C specimens heated to 1700 °C after approximately 1 mm of the surface region had been removed by grinding (Fig. 6). Both these results are different from XRD measurements taken from the specimen surfaces (Fig. 2). Specimen B1-C now shows the presence of some residual $\alpha$-$Al_2O_3$ in the specimen centre, while from the surface XRD data (Fig. 2c) all the $Al_2O_3$ appeared to have been consumed to form mullite. Specimen B1-B shows even greater discrepancy between the specimen interior and specimen surface. In the interior mullite has started to form but there are substantial

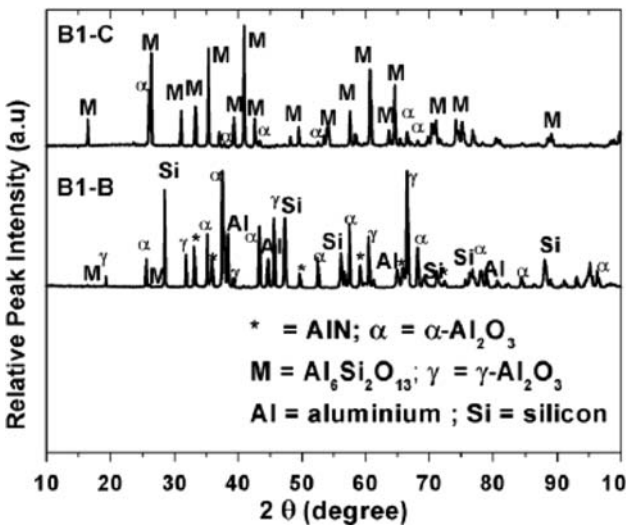


**Fig. 6** XRD traces after surface removal from B1-B and B1-C samples after heating to 1700 °C

quantities of the $\gamma-$ transition alumina, residual Al and Si, and a phase indexed as AlN.

The major differences between the phase composition of the specimen surface and specimen interior can come about through three different mechanisms.

1. Poor mixing of the PMS and Al leading to a heterogeneous distribution of chemical species.
2. Significant thermal lag between the specimen interior and the surface leading to incomplete reaction in the specimen interior.
3. Poor access of the furnace atmosphere to the specimen interior leading to reduced reaction rates or different thermodynamic driving forces in the specimen interior.

In an earlier study of the influence of the Al filler powder morphology on the formation of mullite from Al/PMS mixtures, it was proposed that different powder characteristics strongly influence the porosity of the pre-ceramic compact and that mechanism (3) was hence dominant. Our results here confirm not only the importance of oxygen access, but also illustrate the important role of liquid Al in the intermediate stages of the reaction sequence. From the XRD results from B1-A and B1-B in Fig. 2, it is clear that Si can be retained to very high temperatures along with Al. It is clear from Fig. 7, a BSE image from specimen B1-A heated to 1700 °C, that within the Al rich phase (tentatively identified as metallic Al) there are precipitates of Si. Thus Si is retained to high temperature in solution in liquid Al and the more reactive Al oxidises preferentially. This explains the very large Si crystals found in B1-C (Fig. 4c) as these form by solute rejection as an increasing quantity of the liquid Al is oxidised. The much smaller Si crystals found in B1-A and B1-B are because of their higher Al content and thus Si forms on solidification of the Al-Si alloy. In B1-C, all the Al has oxidised, revealing elemental Si. The presence of excess Al in B1-A and B1-B also explains why the clear endotherm associated with Si melting is only evident in the DSC results from B1-C (Fig. 1).

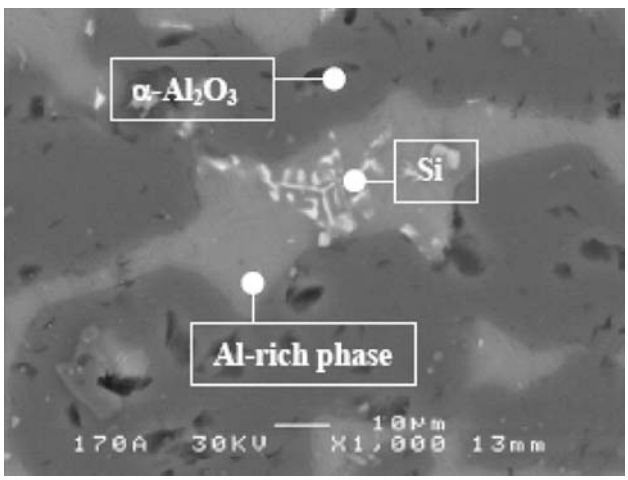


**Fig. 7** BSE SEM image from B1-A heated to 1700 °C

In the micrographs of B1-A and B1-B there is evidence for continuous surface, or sub-surface, layers of $Al_2O_3$ (Fig. 4d and e). These may block the access of O into the specimen interior and explain the large quantity of retained Al in both samples, even after heat treatment to 1700 °C. In B1-B poor access of atmospheric O may have allowed the Al to react with nitrogen, to form AlN after the oxygen had been consumed to form $Al_2O_3$. In an earlier study, a nitrogen containing Sialon phase was found after heat treatment of a stoichiometric Al/PMS mixture to 1700 °C and poor oxygen access was considered to be the responsible for its presence [5]. As yet we have no mechanism to explain the presence of $\gamma$-$Al_2O_3$ in the interior of B1-B, which would have been expected to transform to $\alpha$-$Al_2O_3$ at 1700 °C.

## Conclusions

Varying the composition of Al/PMS mixtures has a strong influence on the phase composition and microstructure of the reaction products achieved by heating Al/PMS mixtures. Altering the Al/PMS ratio does not influence the composition of the resultant mullite phase but it can influence whether mullite forms at all. The Al/PMS reaction route after pyrolysis and heat treatment is complex with intermediate stages of Si, $SiO_2$ or Si–O–C (amorphous), $Al_2O_3$ ($\gamma$- and $\alpha$-), Al-oxycarbides, Al-nitride, Al-silicon carbide and, depending on the ratio of Al/PMS in the initial mixture, can result in the formation of 3:2 stoichiometric mullite. The final reaction product is predominantly mullite if the initial Al/PMS ratio is equivalent to the Al:Si ratio for stoichiometric 3:2 mullite. As the initial mixture becomes more Al rich, the proportion of mullite decreases and for composition B1-A no mullite was detected. The main effect of increasing the Al concentration is to lock elemental Si into solution in liquid Al and reduce its availability to be oxidised. This ensures that the major $Al_2O_3$ phase for reaction to form mullite is $\alpha$-$Al_2O_3$ and that mullite forms at a relatively high temperature by conventional solid-state reaction. A secondary affect of the excess Al is to block the access of atmospheric oxygen to the specimen interior. In the case of specimen B1-B this leads to the formation of AlN.

## References

1. Wei Q, Pippel E, Woltersdorf J, Scheffler M, Greil P (2002) Mater Chem Phys 73:281
2. Scheffler M, Wei Q, Pippel E, Woltersdorf J, Greil P (2002) Key Eng Mater 206–213:289

3. Suttor D, Kleebe HJ, Ziegler G (1997) J Am Ceram Soc 80:2541
4. Anggono J, Derby B (2005) J Am Ceram Soc 88:2085
5. Anggono J, Derby B (2006) J Europ Ceram Soc 26:1107
6. Michalet T, Parlier M, Beclin F, Duclos R, Crampon J (2002) J Eur Ceram Soc 22:143
7. Cameron WE (1977) Am Mineral 62:747
8. Burnham CW (1963) Z Kristal 115:127
9. Fischer RX, Schneider H, Voll D (1996) J Europ Ceram Soc 16:109
10. Scheffler M, Greil P In: Mueller G (ed) EUROMAT 99, Wiley-VCH Verlag GmbH, Weinheim, G, pp 307–311
11. Greil P, Seibold M, Erny T (1992) In: Schmidt H, Hirano K (eds) Microcrystalline ceramic composites by active filler controlled reaction pyrolysis of polymers in materials research symposium, vol 274. MRS, Pittsburgh, pp 155–66
12. Renlund GM, Prochazka S, Doremus RH (1991) J Mater Res 6:2716
13. Schmidt H, Buhler P, Greil P (1995) In: Galassi C (ed) Pyrolytic conversion of poly(methylsiloxane) to silicon (oxy) carbide ceramics in fourth euro ceramics, vol 1. Gruppo Editoriale Faenza Editrice S.p.A., pp 299–306